BULLETIN OF THE POLISH ACADEMY OF SCIENCES
TECHNICAL SCIENCES, Vol. 69(6), 2021, Article number: e139000
DOI: 10.24425/bpasts.2021.139000

A meshless method for subsonic stall flutter analysis of turbomachinery 3D blade cascade

Chandra Shekhar PRASAD*, **Pavel ŠNÁBL, and Luděk PEŠEK**

Institute of Thermomechanics of the CAS, Prague, Czech Republic

Abstract. The analysis of subsonic stall flutter in turbomachinery blade cascade is carried out using a medium-fidelity reduced-order aeroelastic numerical model. The model is a type of field mesh-free approach and based on a hybrid boundary element method. The medium-fidelity flow solver is developed on the principle of viscous-inviscid two-way weak-coupling approach. The hybrid flow solver is employed to model separated flow and stall flutter in the 3D blade cascade at subsonic speed. The aerodynamic damping coefficient w.r.t. inter blade phase angle in traveling-wave mode is estimated along with other parameters. The same stability parameter is used to analyze the cascade flutter resistance regime. The estimated results are validated against experimental measurements as well as Navier-Stokes based high fidelity CFD model. The simulated results show good agreement with experimental data. Furthermore, the hybrid flow solver has managed to bring down the computational cost significantly as compared to mesh-based CFD models. Therefore, all the prime objectives of the research have been successfully achieved.

Key words: stall-flutter; turbomachinery-cascade; reduce-order-model; meshless-method; viscous-inviscid-coupling; boundary-elementmethod.

1. INTRODUCTION

The power turbines are the heart of the majority of electric power generation plants. To address the ever-increasing demand for base energy worldwide, manufacturers are developing and building gigantic power turbines, more specifically steam turbines. The Arabelle turbine manufactured by General electric (GE), of USA has low pressure (LP) stage blade length 1.9 m. According to GE it is used by one-third of the world's nuclear power plants [1]. But these large blades are very much susceptible to flow-induced vibrations due to high aerodynamic loading, longer size and lower stiffness. The flow-induced vibrations can be called flutter and it is a dynamic aeroelastic phenomenon and in the majority of the cases can result in high-cycle fatigue failure, if not addressed well. Therefore, the flutter-free design of LP stage turbine blade continue to be a huge issue among the researchers [2, 3].

In general, there are three common types of flutter in LP stage turbines which have been reported in the past as shown is Fig. 1. In this paper, a study of subsonic stall flutter is the subject of focus. Subsonic stall flutter is one of the dominating and frequently occurring aeroelastic phenomenon in large power turbines. Subsonic stall flutter in steam turbine LP stage is a very complex physical phenomenon and remains a very active topic of research. However, less work has been done in the subsonic dynamic stall flutter in steam turbine cases in the past. The majority of work on subsonic dynamic stall flutter is carried out either on gas turbine or jet engine compressors and

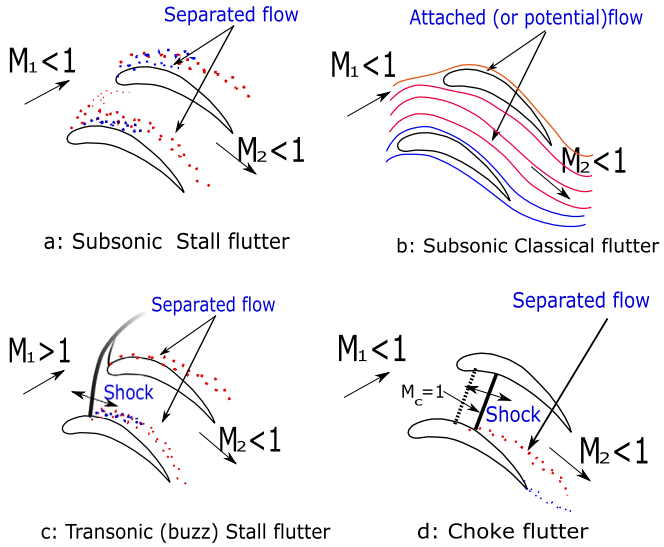

Fig. 1. Steam turbine flutter map

fan blades [4, 5]. Furthermore, in industry numerical tools are preferred over physical models, which can save both time and money to design and develop flutter resistance blade. To numerically study all types of flutter in steam turbines, there are well-developed high-fidelity computational fluid dynamics (CFD) and computational structural dynamics (CSD) based aeroelastic models available. In the past Rządkowski *et al.* [6] used fully viscous CFD approach for stability analysis of 12 blade cascade. However, these CDF-CSD based models are computationally very expensive, therefore, not suited for multiple design iteration computation. Moreover, in CFD-CSD based aeroelastic models, flow computation is responsible for the majority

*e-mail: cprasad@it.cas.cz

Manuscript submitted 2021-03-25, revised 2021-07-12, initially accepted for publication 2021-08-16, published in December 2021

of computational time. Therefore, in this research the issue of subsonic stall flutter is studied in detail. The study will be carried out both experimentally and numerically to understand the fundamental physics behind it. Aerodynamics damping (AD) is one of the parameters to study the aeroelastic stability of stall flutter in 3D blade cascade.

Aim and scope of the research: A cost-effective medium-fidelity hybrid boundary element method (BEM) for flow modeling is developed to study subsonic stall flutter phenomenon in a 3D blade cascade. Therefore, the novelty of the research work lies in the successful development and the implementation of the hybrid BEM type PM flow solver with wall effect to study stall flutter for blade cascades.

For this purpose, unsteady surface panel methods (PM) are employed. PM belongs to the family of BEMs and is well suited for the attached flow problems. The PM was first conceptualized by Hess and Smith [7] to model the lifting and non-lifting potential flow around slender bodies. The PM presents a good trade off between execution speed and accuracy, furthermore, its can also be used for complex geometries in potential flow field.

A study of classical flutter as shown in Fig. 1b in the 2D blade cascade using PM based BEM flow solver is carried out by Prasad *et al.* [8, 9]. In the stall flutter case, the flow is dominated by separated flow, thus classical PM can be used here. However, for subsonic stall flutter a modified version of PM using viscous-inviscid coupling including discrete vortex particle (DVM) wake model can be employed for the separated flow problem [10–12] as it is in stall flutter. Moreover, the equivalent technique is also adopted for aeroelastic modeling of wind turbines [12–14], helicopter rotors, and aircraft aeroelasticity problems [10, 15]. Also the classical BEM-PM was used by the author to model 2D classical flutter analysis in the past [16, 17]. The AD for different Inter blade phase angle (IBPA) for traveling wave mode oscillation is estimated using the proposed hybrid BEM-based flow model. The estimated AD is compared with experimental data and CFD results to evaluate the efficiency and accuracy of the model. The successful implementation of the proposed aeroelastic model for subsonic stall flutter for a 3D cascade will dramatically bring down the computational cost. Also, this will provide an opportunity to researchers and engineers to quickly and efficiently optimize the LP turbine rotor blade geometry for a flutter resistance design with multiple iterations in preliminary design stage.

2. HYBRID REDUCED-ORDER BEM FLOW MODEL

In this section, the development of the reduced-order BEM-based hybrid flow solver is presented. A similar approach is also adopted by Prasad at el. [18] for 2d cascade. The details about the mathematical formulation and the numerical implementation strategy is also discussed in brief.

2.1. Unsteady 3D surface Panel method for flow modeling

3D Surface panel methods are well known to model attached flow problems around lifting and non-lifting surfaces using the potential flow assumptions, which dictates that the flow field is inviscid (Viscosity $(\eta) = 0$) and irrotational ($\nabla \times \vec{V} = 0$). The rectangular singularity panel elements are placed on the entire solid surface and in the wake, these singularity elements are the known solutions to Laplace's equation (1).

$$\nabla^2\Phi(x,y,z) = \frac{\partial^2\Phi}{\partial^2 x} + \frac{\partial^2\Phi}{\partial^2 y} + \frac{\partial^2\Phi}{\partial^2 z} = 0, \tag{1}$$

where $\Phi(x,y,z)$ is the scalar velocity potential which is a function of (x,y,z) such that $(V = \nabla\Phi)$. Apart from singularity distributions appropriate boundary conditions are required to find the unique solution of Laplace's equation. The required BCs are: 1) enforcing the impermeability flow at a solid or fixed normal flow condition ($\nabla\Phi \cdot \mathbf{n} = V_n = 0$). 2) Far field: The disturbance created by the singularities on the body and wake must disappear at infinity ($\lim_{|\mathbf{r}|\to\infty} \nabla(\Phi - \Phi_\infty) = 0$). 3) the Kutta condition and Kelvin's theorem, can be evoked to obtain a full description of the flow field. The pressure field (p) is then obtained solving the unsteady Bernoulli's equation (2)

$$\frac{\partial\Phi}{\partial t} + \frac{p}{\rho} + \frac{V^2}{2} = \text{const}. \tag{2}$$

Furthermore, the original airfoil surface is discretized into smaller surface geometrical panels and the singularity elements are distributed on these panels. In Fig. 2 a discretization scheme of PM is shown, More details about required BC, numerical implementation and determining field variables using the unsteady PM can be found in Katz [19]. Further, to use the PM for internal flows, where the flow field is bounded by solid boundary, the tunnel wall effects can be considered. The strategy to simulate the wind tunnel effect using PM is presented in Fig. 2b, where tunnel walls are distributed with constant strength source elements and the surface normal (n) are oriented inwards as shown in Fig. 2b, this is because the flow of interest is within the tunnel not the outer flow field. More details about wall effect simulation can be found in [20, 21], a similar technique is used here.

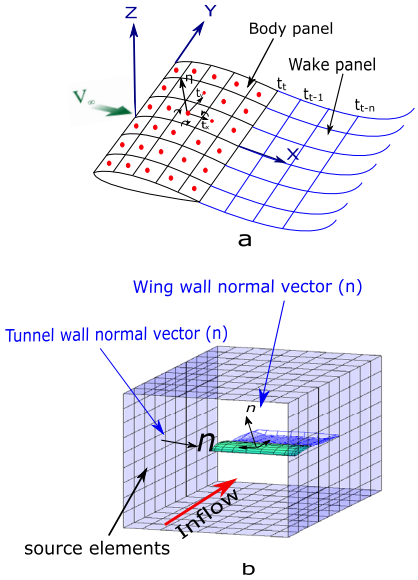

Fig. 2. Panel method discretization scheme (a) and the wind tunnel wall effect approach in internal PM (b)

2.2. Viscous-inviscid coupling and Vorton wake method

Though the PM has many advantages over CFD model, however, there are situations where PM is not suitable compared to CFD. PM incontinence to accurately model the flow separation and account for viscous forces is one of the major drawbacks of classical PM. Therefore, in the current work significant modifications are made in the classical PM formulation to model the flow separation and to account for fluid viscous effect. The modification are made with the help of two-way viscous-inviscid loose coupling strategy. Unlike Prasad *et al.* [22] the one way viscous-inviscid loose coupling model to simulate static flow separation, the present model can also accurately simulate stall flutter cases. This is achieved by calculating time-varying separation points at each time step which makes this method unique compared to other methods proposed in the past. Furthermore, the time varying trailing edge and separated wakes from the airfoil surface are modeled using discrete vortex particle method (DVM), because it is very challenging to represent unsteady stall flutter wake using continuous doublet vortex sheet, also it can introduce severe numerical instability issues. A complete strategy of hybridization of classical PM is presented in Fig. 4.

Furthermore, the separation points are determined using an integral form of 2D BL equations which rely on the *Von kármán momentum integral equation*. The implementation of 2D integral BL solution and wake shedding technique is similar to [22]. However, unlike [22] the separation points are calculated for each time step and a second wake is shed from a new separation point to stimulate stall flutter. A flowchart algorithm of the hybrid flow solver method is shown in Fig. 3. The whole procedure can be described in a step by step manner as follows:

step 1: At the 1th time step ($t = 0$), the inviscid solver (classical PM) is evoked to calculate the inviscid velocity profile over the airfoil/blade along the chordwise position.

step 2: The inviscid velocities calculated in the previous step are transferred to the viscous solver (BL) as input. In the current work 2D BL equation are solved along the chordwise direction only.

step 3: The integral 2D BL is employed to estimate the BL parameters in the chordwise direction starting from the leading edge to the trailing edge on each side. This solution is carried out on all spanwise positions to estimate the separation point. Once the separation point is detected, a nascent doublet panel is shed into the free stream, as shown in Fig. 4c.

step 4: The induced perturbation velocity potential on the entire blade surface exerted by the sounding flow flied is then estimated. Using this perturbation velocity potential, other unsteady aerodynamic field variables, e.g. velocities and pressure are calculated.

step 5: In the next step, the doublet wake panels shed in the previous time step from the trailing edge and the suction side are converted into an equivalent vortex blob as shown in Fig. 4.

step 6: The vortex blobs are then propagated into downstream direction with the local flow velocity. The evolution of these blobs is estimated by employing vorticity transport equation (3). At this point one complete time step ends.

step 7: And the next time step begins with unit increment in the time step indexing and the entire procedure is repeated from step 1.

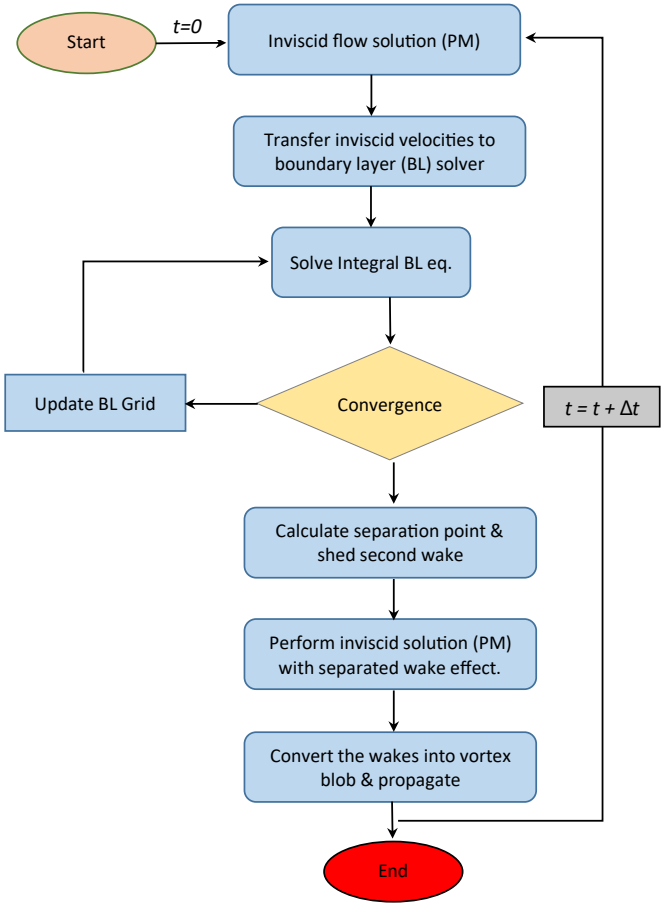

Fig. 3. Flowchart for the hybrid flow solver algorithm

Furthermore, to develop the hybrid flow solver to model unsteady separated flow, some key assumptions are made and can be given as follows:

- It is assumed that the separation only occurs on the suction side at a higher angle of attack. Pressure side separation has a negligible effect, thus not included in the model. Therefore, calculation time can be reduced further.
- The separated shear layer ought to be aligned with streamline, thus there is no static pressure drop across them.
- For the lower incident angle ($aoa \leq 5$), the flow is assumed to be attached throughout the airfoil surface. Therefore, the hybrid PM solver is not evoked instead the classical PM is used. This also reduces the computational time with compromising the accuracy.

2.2.1. Wake modeling using DVM

Once the separation point is known, a doublet shear layer is shed from the separation point and a second one from the trailing edge. The first panel is the nascent wake panel as shown in Fig. 4. In the next time-step the nascent panel is converted into a vorton and a new nascent wake panel is shed again from new

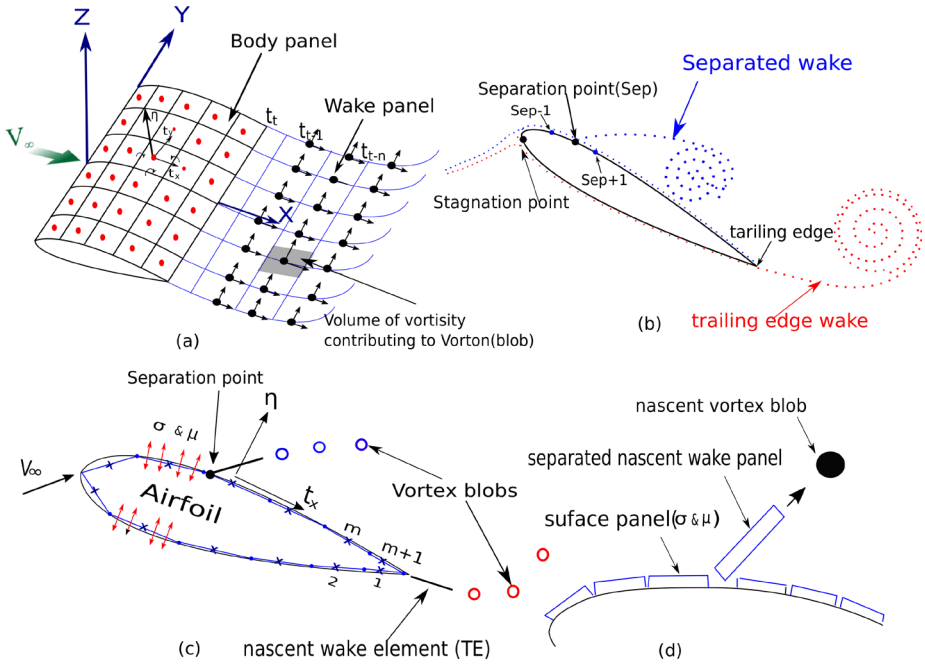

Fig. 4. Concept of separated wake and vortex particle wake conversion and propagation

separation point and the vortons are propagated downstream. In the case of DVM the time-varying motion and evolution of the vortex blobs (Vortons) are estimated using the vorticity transport equation and for the incompressible flow it can be given by euqation (3)

$$\frac{D\omega}{Dt} = (\omega.\nabla)\vec{u} + \nu\nabla^2\omega\,, \tag{3}$$

where ω is vorticity vector, u velocity vector, ν is kinematic viscosity, and ∇^2 is Laplace's operator, respectively. A similar technique to model the unsteady wake is adopted by [11, 12]. The conversion of doublet wake panel into an equivalent vorton is carried out by a similar approach as proposed by [11, 12] to model the unsteady wake. The process continues until the end of time or preset convergence criteria of the aerodynamic forces have been reached.

2.2.2. Pressure correction in separation zone

Only just by shedding second shear layer from the suction side is not enough to model the flow separation. In reality a drop in total pressure may occur across the secondary shear layer. This drop in pressure is assumed to be the main cause of drop in static pressure within the separation zone (between separation point and trailing edge on suction side of the airfoil) drawn in Fig. 4b. Therefore, the modified pressure coefficient formulation for the separation zone can be expressed by equation (4)

$$C_{p_{\text{sep}}} = 1 - \frac{V_t}{Q_\infty} + \frac{\Delta H}{\frac{1}{2}\rho Q_\infty}\,, \tag{4}$$

where V_t is the tangential velocity on the surface and ΔH is the change in total pressure head across the separation line. The value of the pressure drop can be estimated by evoking Bernoulli's equation in the region confined between the separation zone and the free stream zone as proposed by [12]. It can be expressed by

$$\begin{aligned}\Delta H &= \Delta H^- - \Delta H^+ \\ &= \frac{V_t(sep-1,j,t)^2}{2} - \frac{V_t(sep+1,j,t)^2}{2}\,,\end{aligned} \tag{5}$$

where ΔH^- and ΔH^+ are the total pressures above and under the separated wake. Applying the analysis by [23] the pressure coefficient becomes

$$C_{p_{sep}} = 1 - \frac{Vt}{Q_\infty} + \frac{1}{\rho}\left(\frac{\mu_{sep}}{Q_\infty}\right)^2 \tag{6}$$

and the pressure coefficient out of separation zone can be given as

$$C_p(x,y,t) = 1 - \frac{V_{\text{total}}^2}{V_\infty^2} - \frac{2}{V_\infty^2}\frac{\partial\mu}{\partial t}\,, \tag{7}$$

where V_{total} is the sum of the local kinematic velocities and the singularity induced velocity.

3. FLUTTER ANALYSIS METHOD

The aeroelastic equation which represents the equilibrium between the structural and aerodynamic forces of the whole system can be expressed by equation (8)

$$[\mathbf{M}]\{\ddot{\vec{X}}\} + [\mathbf{G}]\{\dot{\vec{X}}\} + [\mathbf{K}]\{\vec{X}\} = \{\vec{F}_{ab}(t)\} \tag{8}$$

where the $[\mathbf{M}]$ modal mass matrix, $[\mathbf{G}]$ damping matrix, and $[\mathbf{K}]$ stiffness matrix. The modal is a coordinate vector represented by $\{\vec{X}\}$ and $\{\vec{F}_{ab}(t)\}$ is the modal unsteady aerodynamic

force vector. The unsteady aerodynamic force vector is a combined effect of $\vec{F}_{\text{disturbance}}(t)$ that includes the aerodynamic disturbances upstream and downstream the blade and $\vec{F}_{\text{damping}}(t)$ which represents the aerodynamic damping resulting from the interaction between the blade itself and the flow. Furthermore, it is assumed that there is negligible disturbance in the upstream and downstream flow, thus $\vec{F}_{\text{disturbance}}(t) = 0$ therefore, equation (8) simplifies to

$$[\mathbf{M}]\{\ddot{\vec{X}}\} + [\mathbf{G}]\{\dot{\vec{X}}\} + [\mathbf{K}]\{\vec{X}\} = \vec{F}_{\text{damping}}(t)\} \tag{9}$$

and equation (9) can be used to the determine the aerodynamic damping of the system and the aeroelastic stability of the system.

The most common approach to estimate the unsteady aerodynamic forces for such a system is "Time Linearized Method (TLM)" and it is adopted by several researchers in this field. In the TLM approach, it is assumed that the unsteady perturbations in the flow are small compared to the mean flow. Therefore, the unsteady flow can be represented by small harmonic perturbations around a mean value.

In this research work, hybrid PM is used as TLM to estimate the unsteady aerodynamic forces. Furthermore, TWM method with the principle of linear superimposition is adopted to determine the AD [24,25]. In the cascade the aerodynamic influence of the main blade on which the damping is evaluated and the influence of other blades on it is superimposed to get the total aerodynamic damping. Therefore, in TWM the total unsteady response on a blade (here blade "0" in Fig. 5) is composed of the individual responses from itself and from the other blades lagged by the respective multiple of the IBPA. This effect can be given by equation (10)

$$\hat{c}^{m,\sigma}_{P,h,twm}(x,y,z) = \sum_{n=-N/2}^{n=+N/2} \hat{c}^{n,m}_{P,h,ic}(x,y,z).e^{-i\sigma.n}, \tag{10}$$

where $\hat{c}^{m,\sigma}_{P,h,twm}(x,y,z)$ represents the complex pressure coefficient at point (x,y,z), acting on blade m with the cascade oscillating in traveling-wave mode with IBPA σ and $\hat{c}^{n,m}_{P,h,ic}(x,y,z)$ is the pressure coefficient of the vibrating blade n, acting on the non-vibrating reference blade m at point (x,y,z). The coefficients $\hat{c}^{n,m}_{P,h,ic}(x,y,z)$ are commonly referred to as local aerodynamic influence coefficients and are normalized by dynamic pressure "q" and amplitude of oscillation "h". The pressure coefficient is integrated over the surface to get the unsteady force. The work done in each cycle is obtained by multiplying the total force with the respective oscillating displacement which can be given by equation (11)

$$W_{\text{cycle}} = \int_{t_0}^{t_0+T} \int_{A} -p.\vec{V}.\vec{n}.\mathrm{d}A\,\mathrm{d}t = \int_{T} \hat{\vec{F}}.\hat{\vec{h}}.e^{i\omega t}\,\mathrm{d}t, \tag{11}$$

where $\hat{\vec{h}}$ is the complex motion of the cascade blade and A the surface area of the blade. For this research work pitching motion of the cascade blade is analyzed, which corresponds to torsional motion. The torsional flutter AD coefficient can be determined from the work done per cycle normalized by π and the amplitude of oscillation "h" as given in equation (12)

$$\textit{Aerodynamic damping}(\Xi) = -\frac{W_{\text{cycle}}}{\pi h^2}, \tag{12}$$

where W_{cycle} is the aerodynamic work done per cycle. The *Positive* values of Ξ indicate that the flow is acting in a stabilizing manner whereas *Negative* values can cause flutter and are therefore, considered unstable.

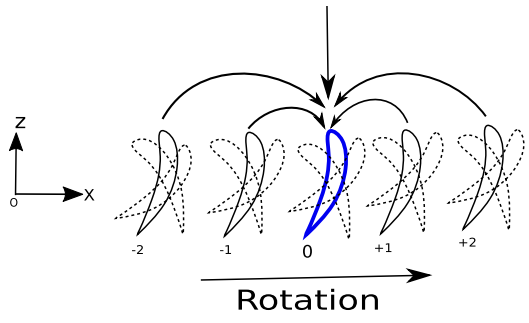

Fig. 5. Indexing of blades in cascade and traveling wave mode oscillation

4. EXPERIMENTAL SETUP FOR 5 BLADE CASCADE

The physical model of the blade cascade is shown in Fig. 6. Five 3D printed blades with NACA0010 profile and 70 mm chord length and 100 mm span are attached to the base plate. The base plate can be rotated to set the desired angle of attack (α), each blade can also slide horizontally to set the stagger angle of the cascade. Each of the five blades is attached to the base plate

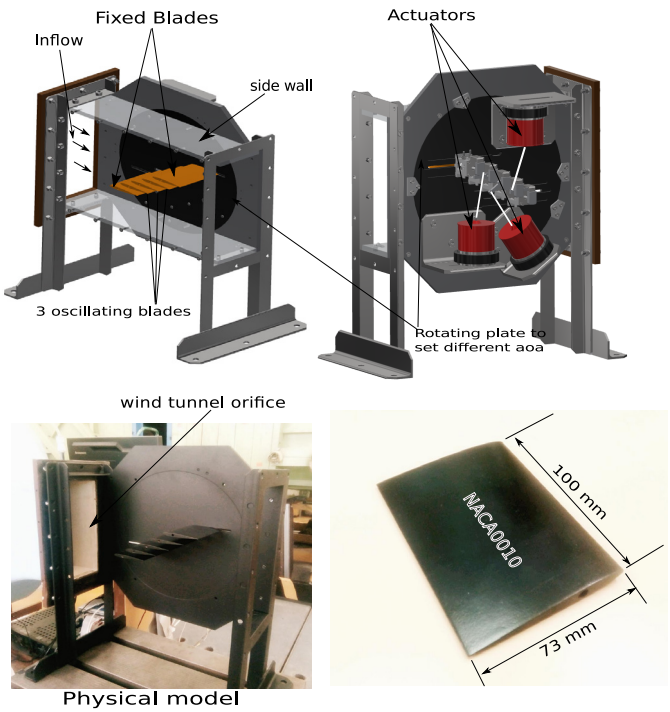

Fig. 6. Experimental setup and physical model of the 5 blade cascade

with a mechanism which allows for the individual excitation. The experiment is performed in two different configurations. In one configuration the two end blades (–2 and +2 blade number) in Fig. 7 are fixed and the three blades 0, –1 and +1 are excited with the help of a shaker, the position of the shakers is shown in the top right in Fig. 6. All the blades are placed inside a rectangular channel with one flow inlet from wind tunnel and the exit as shown in Fig. 6. The gap between the channel walls and the blade tip is negligible to ensure the 2D flow field over the cascade and minimize the tip vortex effects. In the second configuration, all the blades hang and are free to move in pitching motion. They are suspended with the help of torsional springs. The experimental test campaign is carried out for a wide range of different flow speeds from 10 m/sec to 50 m/s, different flow angles (from 0° to 15°) and stagger angles (from 10° to 25°). The aerodynamic damping is estimated by multiplying the total force with the total pitching displacement in one cycle of oscillation. A similar experiment on NACA0010 blade cascade is also carried by Tsymbalyuk *et al.* [26].

Table 1
Flow parameters

Parameter	Value
Chord (C)	73 mm
Flow angle (α)	$+5°to+15°$
Stagger angle (β)	$+15°to+25°$
Slant height (τ)	18 mm
Oscillating feq. (ω)	10 Hz to 30 Hz
Oscillating Amp. ($\bar{\alpha}$)	± 2 mm to ± 5 mm

The experimental test is carried out on a 5-blade cascade with NACA0010 series airfoil and flow conditions are constant inlet velocities 10 m to 40 m/sec, mean camber line incidence angles ($\alpha_0 = 5°$ to 15°), pitching amplitudes ($\bar{\alpha} = 2°$ to 5°), reduced frequencies $k = 0.015$ to 0.3 based on semi chord, and 18 IBPA (φ) = 0, ±180° with 20° interval. This kind of superimposed velocity potential can be obtained for any airfoil in the cascade.

The oscillatory motion of the cascade blade can be given in complex form by

$$\alpha(t) = \bar{\alpha} e^{i(\omega t \pm n\varphi)}, \tag{13}$$

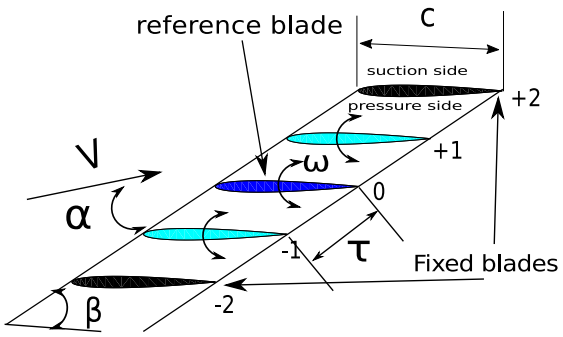

Fig. 7. Schematic diagram of and nomenclature of cascade

where n is blade number Fig. 7 and the ω is the frequency of oscillation in rad/sec and $\omega = \dfrac{2.k.U_\infty}{chord}$. Hence the effective angle of attack (α_{eff}) at any time instance is given by equation (14)

$$\begin{aligned}\alpha_{\text{eff}}(t) &= \alpha_0 + \alpha(t) \\ &= \alpha_0 + \bar{\alpha} e^{i(\omega t \pm n\varphi)} = \alpha_0 + \bar{\alpha}\sin(\omega t \pm n\varphi).\end{aligned} \tag{14}$$

The blade cascade and geometry and the related parameter values are given in Fig. 7.

5. CASCADE FLUTTER ANALYSIS WITH UNSTEADY PM

To construct the flow field around the oscillating cascade as shown in Fig. 7 using the hybrid PM solver, each cascade is discretized into small number of panels. Constant strength source and doublet singularity elements are distributed over the discretized airfoils, and the free wake is modeled using DVM. In order to evaluate the aerodynamic damping at reference airfoil ("0") the velocity potential (Φ) induced by the source and the doublet singularity element of the airfoil and the all the other airfoils oscillating in the respective phase lag are superimposed linearly including the effect of free wakes. This is arranged in matrix form and called aerodynamics influence coefficient matrix (AICM). Using AICM along with zero normal flow on the body wall, the system of equations $[A]\{x\} = \{y\}$ can be solved to estimate the unknown strength of the perturbation potential. More details about this numerical calculation are given in Katz [19] and the same formulation is adopted here. Once the perturbation potential is known, the unsteady pressure coefficient can easily be estimated, hence the aerodynamic force and the work for each time step is the summation of all the time steps in one complete cycle giving the total aerodynamic work done in one period. The wake shape and flow field around the cascade simulated using hybrid PM is presented in Fig. 8. The evaluation of the flow field is depicted after 25 time steps the time step size is $\delta t = 0.0025$ sec. and oscillating frequency is 21 Hz with an amplitude of oscillation of 3 degrees and inflow angle of 10 degrees and $k = 0.115$. The flow starts to separate

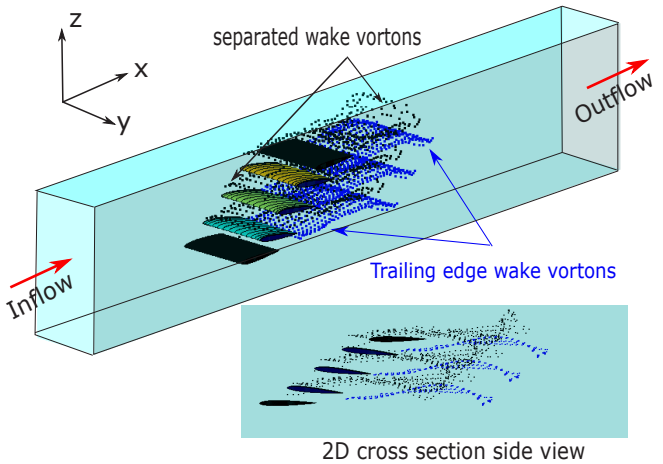

Fig. 8. Vorton wake shapes after time step = 25 using hybrid PM at $\alpha_0 = 10°$ and $\bar{\alpha} = 3°$ at reduced frequency $k = 0.115$ and wind speed $Q_\infty = 40.0$ m/s; Pure torsional flutter at 0 IBPA

from the suction side of the all airfoils, but the separation position varies in the three oscillating airfoils depending upon the oscillation cycle. In Fig. 8, the suction side separated wakes are depicted in "black" color vorton and the trailing edge wakes are in "blue". Due to visualization reasons only wakes from the oscillating blade are plotted in the picture. Furthermore, from convergence point of view the proposed hybrid PM performs very well and starts to converge after 50 time steps for both test cases. Also, the fast convergence is due to the fact that PM is based on Laplace's potential flow equation, which is a second order linear differential equation, therefore, the solution starts to converge as soon as starting vortices move away from the body. For the present test cases it starts around 50th time step.

6. CASCADE FLUTTER ANALYSIS USING CFD MODELS

To evaluate the efficiency and the accuracy of the hybrid-PM model in comparison to Navier–Stokes (NS) based CFD models, a stability analysis of the 5 blade cascade setup is carried out using CFD numerical models. For the stability analysis the AD curve for the cascade (for reference blade) is estimated using both viscous and inviscid CFD models. The CFD modeling is performed in ANSYS/Workbench 2020R environment. The entire flow domain is discretized using finite volume (FV) mesh elements. The complete mesh strategy for the numerical discretization of the whole domain is shown in Fig. 9. For the better visibility coarse mesh is shown here, but in calculation more finer converged mesh is used. The inner deformable zones are discretized into O-type structured grid elements, whereas non-deforming zone is discretized into unstructured quadrilateral FV elements. A similar O-type inner grid is also used by Rządkowski *et al.* [6, 27] for 2D cascade simulation using viscous flow CFD-models. For inviscid modeling, the inviscid version of NS-equation (or Euler equation) for the compressible flow is used and the viscous modeling is carried out using SST $K-\omega$ RANS model with refined BL mesh to make sure the Y^+ value remains below 1. The total numbers of grid elements are 0.21 million and it was achieved after grid convergence tests. The estimated AD using viscous and inviscid CFD models are compared to the PM-hybrid and experimental AD in Fig. 11.

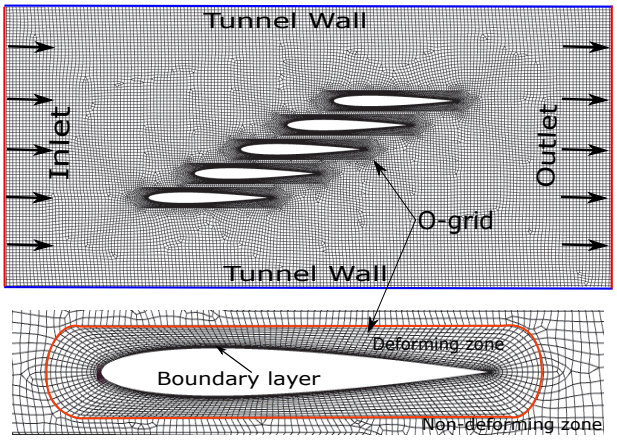

Fig. 9. CFD-mesh strategy: O-type inner structured grid, quadrilateral outer unstructured grid

7. RESULTS

At first, the the isolated pitching airfoil test is selected for comparison purpose. The experimental results are obtained from Galbraith *et al.* [28]. A cyclic lift coefficient of the NACA0015 test results, which correspond the stall flow condition, is compared to simulated results using hybrid PM and presented in Fig. 10. In Fig. 10 estimated results from the present numerical model have good agreement with the experimental data, although they exhibit a slight overestimation of the lift for a high angle of attack (above 15°).

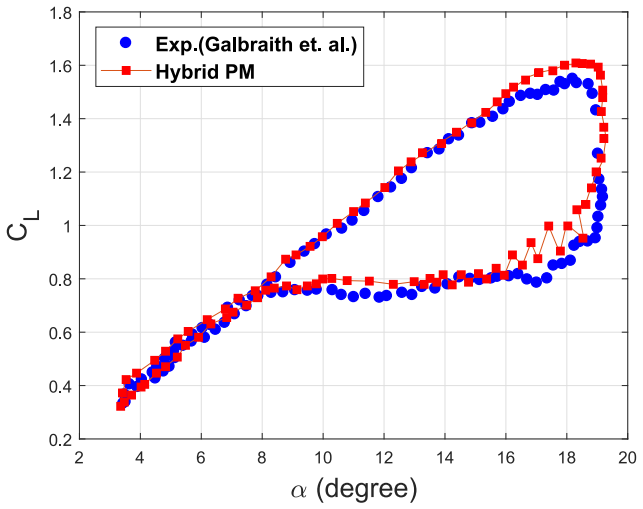

Fig. 10. Lift coefficient vs. angle of attack for pitching aerofoil NACA 0015 at Re =1.5×10^{06}, reduced frequency (k) = 0.05

A small deviation in the shape of the C_L loop can be detected in the region close to the maximum pitching angle during the downstroke. This can be caused by a strong separated vortex originated due to downstroke motion of the airfoil at the peak maximum angle. Furthermore, the present numerical results exhibit some oscillations when the stall occurs (between 13° and 18°) which is caused by the accumulation of vortex blob at one point of time which may induce strong velocity potential on the airfoil surface. The problem can be solved by using a more sophisticated diffusion method or eliminating some blobs during this period. Furthermore, it is worth mentioning that the computation time taken to get converged result for this pitching airfoil is approximately 3 (CPU mins) on a single core CPU Intel-i7, which is significantly lower than CFD based model for same test case.

The same hybrid PM is then employed to estimate the aerodynamic stability (AD) for the 5 blade cascade model Fig. 6 and the estimated AD vs. IBPA with error scale w.r.t experimental data is presented in Fig. 11. The hybrid PM estimated stability parameters (AD) are close to the experimental and the CFD results. However, the reduced-order hybrid PM solver overestimates the magnitude of AD value around the peak regions of the AD in both, the stable and the unstable region. The error scale of the hybrid-PM shows the difference in the values between measured and estimated results for different IBPA. The difference in magnitude of AD values is particularly higher in the stable region. Furthermore, the present solver underestimates

the AD value at 0 IBPA compared to experimental data. Experimental data and the both CFD-models estimated data indicates stable motion at 0 IBPA for the given flow condition, whereas, the PM estimation is slightly under stability limit line (0). One can argue that the hybrid PM is a medium-fidelity model for separated flow simulation and cannot capture the unsteady flow field. Strong vortex blade interaction is very sensitive in high frequency stall flutter condition, therefore, it slightly over- or underestimated the stability parameter. Moreover, the discrepancy between experimental and simulated results can be caused by the linear-superimposition principle which cannot handle the stall flutter case effectively. Though the k value is low, the flow field is highly nonlinear due to flow separation, thus, hybrid PM based on linear superimposition principle to account for the effects of neighboring blades might fail to describe it accurately. Furthermore, the viscous CFD results have very close agreement with the experimental AD values for all IBPA, whereas inviscid CFD shows slight overestimation around the peak magnitude regions of the stable and the unstable zone and these difference magnifies for $+130^\circ$ to $+180^\circ$ and -180°, just like PM results . However, the differences are not as large as yielded by hybrid PM in those regions. Also it can be observed that the inviscid AD curve is more closely aligned to the hybrid PM AD curve in compared to the viscous CFD AD curve in Fig. 11. This trend indicates that there exists a strong separated flow vortex interaction within the surrounding flow field which is hard to capture accurately even with high fidelity CFD-inviscid models. Furthermore, both the CFD models take approximately 3 (inviscid) to 4 (viscous) CPU hours on 6 core intel i7 processors to converge for each IBPA, and therefore, 57 CUP hrs (inviscid) to 76 CUP hrs (viscous) for complete AD s-curve. Nevertheless, the over all qualitative accuracy of the simulated AD curve is satisfactory while comparing to experimental data. Furthermore, present proposed method takes approximately 12 CPU mins to estimate the AD s-curve as shown in Fig. 11, which is arguably much lower than computation time needed by Navier–Stokes-based CFD models. However, the CFD model estimation can be more accurate compared to the hybrid PM, because flow separation effects can better be captured by RANS turbulence models in CFD-based numerical models, but computational time will be much higher perhaps over 50 times higher than in the present method. Hence, the present method can be good compromise of speed and accuracy compared to CFD-based models for the subsonic stall flutter analysis.

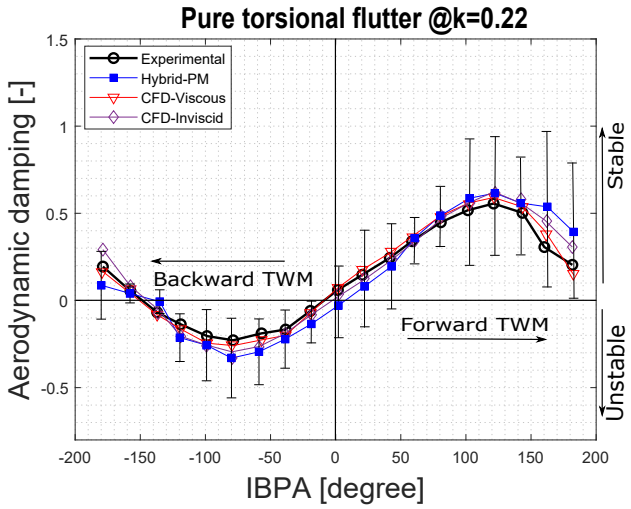

Fig. 11. The AD (Ξ) vs IBPA, at $\alpha_0 = 10^\circ$ and $\bar{\alpha} = 3^\circ$ at reduced frequency $k = 0.115$ and wind speed $Q_\infty = 40.0$ m/s using hybrid PM; pure torsional flutter

8. CONCLUSION

The issue of post-critical aeroelastic stability problem in the turbomachinery blade cascade in 3D configuration is researched here with the help of a medium-fidelity reduced-ordered aeroelastic model (ROAM). The ROAM flow solver is developed on the concept of meshless hybrid BEM family unsteady PM for flow modeling. To model separated flow, the classical panel method is modified using viscous-inviscid coupling technique and the free wake is modeled using discrete vortex particles. The reduced-order hybrid unsteady PM is first tested for a benchmark problem for isolated pitching airfoil test. The estimated cyclic lift coefficient vs angle of attack results are compared with experimentally measured lift coefficients. The numerically estimated result shows good agreement with experimental data, and a significant reduction in computational time compared to high fidelity field-based CFD type model.

In the next steps the reduced-order hybrid PM is employed for post critical aeroelastic stability analysis for subsonic stall flutter in the linear five-blade cascade. The experimental and the simulated AD vs IBPA results are very close for a given flow condition. However, a slight discrepancy is observed between the simulated and the experimental AD curve. This discrepancy in simulated results can be caused by the assumptions made in the hybrid model. In the current hybrid PM models the separation points are estimated using 2D BL formulation, and not including viscous diffusion in the wake model. This might have an effect on the unsteady pressure field in the cascade. Therefore, the results can be further improved by incorporating the viscous diffusion model in DVM and the use of a 3D BL layer model for viscous part. But with these improvements, the computational time will increase significantly. The hybrid PM model results are also compared to the inviscid and viscous CFD models and it is observed that the hybrid PM is significantly faster and accuracy is quite satisfactory, being a medium-fidelity model. Therefore, in the perspective of medium-fidelity model, the over all qualitative results for cascade stability are very satisfactory and the hybrid PM model can be used for the preliminary design stage without significantly compromising the accuracy. Also, it can be better trade off between computational speed and accuracy compared to high fidelity CFD-based RANS model. Therefore, the present subsonic stall flutter analysis approach in blade cascade can have a great potential for industrial applications.

FUTURE WORK

In the future the current numerical will be further improved to include viscous diffusion of vortex particles, also the mild compressibility effect will be added in the solver.

ACKNOWLEDGEMENTS

This research is supported by the Czech Science Foundation (GAČR) Grant-No.20–26779S "Study of dynamic stall flutter instabilities and their consequences in turbomachinery application by mathematical, numerical and experimental methods".

REFERENCES

[1] "Nuclear power: 2 largest steam turbine ever made," 2020, (Accessed: 2020-10-06). [Online]. Available: https://www.ge.com/news/reports.

[2] T. Rice, D. Bell, and G. Singh, "Identification of the stability margin between safe operation and the onset of blade flutter," *J. Turbomach.*, vol. 131, no. 1, 2009, doi: 10.1115/1.2812339.

[3] J. Kiciński, "The flutter effect in rotating machines," *Bull. Pol. Acad. Sci. Tech. Sci.*, pp. 195–207, 2004.

[4] M. Vahdati, N. Smith, and F. Zhao, "Influence of Intake on Fan Blade Flutter," *J. Turbomach.*, vol. 137, no. 8, 08 2015, doi: 10.1115/1.4029240.

[5] J.D. Jeffers and C.E. Meece Jr, "F100 fan stall flutter problem review and solution," *J. Aircr.*, vol. 12, no. 4, pp. 350–357, 1975, doi: 10.2514/3.44454.

[6] R. Rządkowski, V. Gnesin, and L. Kolodyzhnaya, "3d viscous flutter of 11th configuration blade row," *Adv. Vib. Eng.*, vol. 8, no. 3, pp. 213–228, 2009. [Online]. Available: https://www.elibrary.ru/item.asp?id=27911163.

[7] J.L. Hess, "Calculation of potential flow about arbitrary threedimensional lifting bodies," Naval Air Systems Command, Department of the Navy, Final Technical Report MDC J5679-01, 1972. [Online]. Available: https://apps.dtic.mil/sti/citations/AD0755480.

[8] C.S. Prasad and L. Pešek, "Efficient prediction of classical flutter stability of turbomachinery blade using the boundary element type numerical method," *Eng. Anal. Boundary Elem.*, vol. 113, pp. 328–345, 2020, doi: 10.1016/j.enganabound.2020.01.013.

[9] C.S. Prasad, R. Kolman, and L. Pešek, "A cost effective approach for subsonic aeroelastic stability analysis of turbomachinery 3d blade cascade. A reduced order aeroelastic model numerical approach," *Nonlinear Dyn.:under-review*, 2021, doi: 10.21203/rs.3.rs-252660/v1.

[10] V.A. Riziotis and S.G. Voutsinas, "Dynamic stall modelling on airfoils based on strong viscous-inviscid interaction coupling," *Int. J. Numer. Methods Fluids*, vol. 56, pp. 185–208, 2008, doi: 10.1002/fld.1525.

[11] N.R. García, A. Cayron, and J.N. Sørensen, "Unsteady double wake model for the simulation of stalled airfoils," *J. Power Energy Eng.*, vol. 3, pp. 20–25, 2015. doi: 10.4236/jpee.2015.37004.

[12] A. Zanon, P. Giannattasio, and C.J. Simão Ferreira, "A vortex panel model for the simulation of the wake flow past a vertical axis wind turbine in dynamic stall," *Wind Energy*, vol. 16, no. 5, pp. 661–680, 2013, doi: 10.1002/we.1515.

[13] C. Prasad, Q.-Z. Chen, O. Bruls, F. D'Ambrosio, and G. Dimitriadis, "Aeroservoelastic simulations for horizontal axis wind turbines," *Proc. Inst. Mech. Eng., Part A: J. Power Energy*, vol. 231, no. 2, pp. 103–117, 2016, doi: 10.1177/0957650916678725.

[14] C. Prasad, Q.-Z. Chen, O. Bruls, F. D'Ambrosio, and G. Dimitriadis, "Advanced aeroservoelastic modeling for horizontal axis wind turbines," in *Proceedings of the 9th International Conference on Structural Dynamics, EURODYN 2014*, Porto, Portugal, July 2014, pp. 3097–3104.

[15] Z. Goraj, A. Frydrychewicz, R. Świtkiewicz, B. Hernik, J. Gadomski, T. Goetzendorf-Grabowski, M. Figat, S. Suchodolski, and W. Chajec, "High altitude long endurance unmanned aerial vehicle of a new generation – a design challenge for a low cost, reliable and high performance aircraft," *Bull. Pol. Acad. Sci. Tech. Sci.*, pp. 173–194, 2004.

[16] C.S. Prasad and L. Pešek, "Analysis of classical flutter in steam turbine blades using reduced order aeroelastic model," in *The 14th International Conference on Vibration Engineering and Technology of Machinery (VETOMAC XIV)*, Lisabon, Portugal, Sept 2018, pp. 150–156, doi: 10.1051/matecconf/201821115001.

[17] C.S. Prasad and L. Pešek, "Classical flutter study in turbomachinery cascade using boundary element method for incompressible flows," in *Advances in Mechanism and Machine Science*, T. Uhl, Ed. Cham: Springer International Publishing, 2019, pp. 4055–4064, doi: 10.1007/978-3-030-20131-9_404.

[18] C.S. Prasad and L. Pešek, "Subsonic stall flutter analysis in 2d blade cascade using hybrid boundary element method," in *In Proceedings of the 11th International Conference on Structural Dynamics, EURODYN 2020*, Athens, Greece, November 2020, pp. 213–224.

[19] J. Katz and A. Plotkin, *Low-Speed Aerodynamics*, 2nd ed. Cambridge University Press, 2001.

[20] T. Wang and F.N. Coton, "Numerical simulation of wind tunnel wall effects on wind turbine flows," *Wind Energy: An International Journal for Progress and Applications in Wind Power Conversion Technology*, vol. 3, no. 3, pp. 135–148, 2000, doi: 10.1002/we.35.

[21] D. Ashby and D. Sandlin, "Application of a low order panel method to complex three-dimensional internal flow problems," NASA Contractor report 177424, Tech. Rep., 1986. [Online]. Available: https://ntrs.nasa.gov/citations/19860021529.

[22] C.S. Prasad and G. Dimitriadis, "Application of a 3d unsteady surface panel method with flow separation model to horizontal axis wind turbines," *J. Wind Eng. Ind. Aerodyn.*, vol. 166, pp. 74–89, 2017, doi: 10.1016/j.jweia.2017.04.005.

[23] A. Zanon, P. Giannattasio, and C.J. Simão Ferreira, "A vortex panel model for the simulation of the wake flow past a vertical axis wind turbine in dynamic stall," *Wind Energy*, vol. 16, no. 5, pp. 661–680, 2013.

[24] Y. Hanamura, H. Tanaka, and K. Yamaguchi, "A simplified method to measure unsteady forces acting on the vibrating blades in cascade," *Bull. JSME*, vol. 23, no. 180, pp. 880–887, 1980, doi: 10.1299/jsme1958.23.880.

[25] E.F. Crawley, "Measurements of aerodynamic damping on the mit transonic rotor," Cambridge, Mass.: Gas Turbine & Plasma Dynamics Laboratory, Massachusetts Institute of Technology, Tech. Rep., 1981. [Online]. Available: http://hdl.handle.net/1721.1/104728.

[26] V. Tsymbalyuk and J. Linhart, "Corrections of aerodynamic loadings measurement on vibrating airfoils," in *XVII IMEKO World Congress, Dubrovnik, Croatian Metrology Society*. Citeseer, 2003, pp. 358–361.

[27] *3D Viscous Flutter in Turbomachinery Cascade by Godunov-Kolgan Method*, ser. Turbo Expo: Power for Land, Sea, and Air, vol. Volume 5: Marine; Microturbines and Small Turbomachinery; Oil and Gas Applications; Structures and Dynamics, Parts A and B, 05 2006, doi: 10.1115/GT2006-90157.

[28] R. Galbraith, M. Gracey, and E. Leith, "Summary of pressure data for thirteen aerofoils on the university of Glasgow's aerofoil database," *GU Aero report-9221 University of Glasgow*, 1992.